RSC Advances

PAPER

View Article Online
View Journal | View Issue

Cite this: *RSC Adv.*, 2024, **14**, 21219

Aliphatic hyperbranched polyphosphate: a novel multicolor RTP material with AIE character†

Lianlian Wang *[a] and Hongxia Yan [b]

Long-lived photoluminescent probes are emerging as significant luminogens for biological imaging. However, currently, most long-lived luminescent materials contain expensive rare elements or cytotoxic bulky aromatic or conjugated units. Herein, a novel hyperbranched polyphosphate (HBPPE) was synthesized using triethyl phosphate (TEP) and ethylene glycol (EG) through a transesterification polycondensation reaction. The obtained HBPPE P1 can emit bright blue photoluminescence under UV light and show significant AIE character. Interestingly, the average photoluminescence lifetime of P1 is 12.82 μs. This suggests the first phosphorescent material without rare elements or aromatic structures attributed to the covalent-crystal-like structure. Besides, P1 shows an obvious red-shift along with the excitation wavelength, which emits blue, cyan, green, yellow and red photoluminescence, covering nearly all the visible light region. This study not only enriches the species of nonconventional multicolor AIE luminogens but also provides a concise method for the synthesis of HBPPE and demonstrates the possibility for phosphorescent materials without rare elements or bulky aromatic units.

Received 26th April 2024
Accepted 23rd June 2024

DOI: 10.1039/d4ra03099k

rsc.li/rsc-advances

Introduction

Thermally-activated delayed fluorescence (TADF) emitters and room-temperature phosphorescent (RTP) materials are emerging as significant photoluminescent materials for biological imaging as the signals can be easily separated from endogenous fluorophores in time.[1–3] However, it is noted that TADF materials are undoubtedly affected by oxygen, which makes them unsuitable for biological imaging in time.[4,5] Besides, up to now, nearly all RTP materials contain high-cost rare earth elements[6,7] or cytotoxic aromatic building blocks.[8–10] These disadvantages immensely limit the application of TADF and RTP materials in biological imaging. Regrettably, up to now, there has been rarely any report on all organic TADF and RTP materials without bulky aromatic or conjugated units.

In the past nearly two decades, aggregation-induced emission (AIE) has drawn considerable attention owing to its excellent optical properties.[11–13] Nonconjugated AIE materials, without aromatic structures are more biocompatible and environmentally friendly, which make them more suitable for biological imaging and medical applications.[14,15] To date, hyperbranched polysiloxanes,[16–18] poly(amino ester)s,[19,20] poly(ether amide)s[21] and polyacrylonitrile[22] have been reported with AIE character. However, compared with species-rich conventional AIE materials, nonconventional AIE materials still suffer from the lack of species. Moreover, all organic conjugated AIE materials with RTP character have attracted considerable interest and offered extensive advanced applications. Nonetheless, there is nearly no report on nonconjugated AIE materials with RTP character.

Polyphosphates (PPEs), whose structures are similar to lipid bilayers in cells,[23] have attracted considerable attention owing to their potential application in the biomedical field due to their easily implemented functionalization on the side chain, adjustable physicochemical properties, good biocompatibility and biodegradability.[24–26] To date, the most common synthesis of PPE is through polycondensation using phosphoryl halide and polyol or polyphenol.[27–29] The by-product hydrogen chloride is removed by an additional reagent, which complicates the synthesis process. Besides, PPEs can be synthesized by olefin metathesis polymerization[30–32] or ring-opening polymerization of cyclic phosphate monomers.[33–35] These two methods require the use of toxic or expensive catalysts such as Grubbs catalyst or Sn(Otc).[33–35] This complicates the industrial production of PPEs, which limits their use in both flame retardant and biomedical applications. Simple and inexpensive synthesis of polyphosphates plays a pivotal role in achieving a wide range of applications of PPEs. Hence, the development of a novel strategy to prepare PPEs is highly desirable due to the significant shortcomings.

In this study, we synthesized a novel kind of hyperbranched PPE (HBPPE) through a facile one-pot transesterification reaction. Surprisingly, the obtained HBPPE (P1) can emit bright blue photoluminescence under UV light with a quantum yield of up to 22.4% and an average photoluminescence lifetime of 12.82 μs, suggesting the first RTP material without the aromatic structure.

[a]*Chengdu Aeronautic Polytechnic, Chengdu, 610100, China. E-mail: 1435899566@qq.com*

[b]*Northwestern Polytechnical University, Xi'an 710129, China*

† Electronic supplementary information (ESI) available. See DOI: https://doi.org/10.1039/d4ra03099k

Besides, P1 shows obvious AIE character and a red-shift along with the excitation wavelength, emitting blue, green, yellow and red photoluminescence, covering nearly all the visible light region. The reference polymer P2 and P3, transmission electron microscopy and theoretical calculations reveal that the photoluminescence is attributed to the formed covalent-crystal-like structure. This research not only enriches the species of AIE materials but also provides a concise method for the synthesis of HBPPA and a possibility of all organic nonconventional RTP AIE materials.

Experimental section

Materials and methods

Ethanol (EA, AR), methyl alcohol (MA, AR), ethylene glycol (EG, AR) and glycerol (Gl, AR) were supplied by Guangdong Guanghua Sci-Tech Co., Ltd. Triethyl phosphate (TEP, AR) and dimethyl phosphonate (DEP) were purchased from Shanghai Macklin Biochemical Co., Ltd. Regenerated cellulose (RC) dialysis membranes with the molecular weight cut off (MWOC) of 1000 was obtained from Xi'an Yobios Biotechnology Co., Ltd. The RC dialysis membranes were cut off and boiled in distilled water for 15 minutes. Other materials were used without further purification. The nuclear magnetic resonance spectrum (^{1}H NMR, ^{31}P NMR) was recorded on a Bruker Avance 400 MHz superconducting Fourier digital NMR spectrometer using dimethyl sulfoxide (DMSO-d_6) as the solvent. Fourier transform infrared spectroscopy (FTIR) was detected on a Bruker infrared spectrometer with a wavenumber ranging from 4000 to 400 cm^{-1}. Ultraviolet-visible (UV-vis) absorption spectroscopy was measured using a HITACHI U-3900H UV-visible absorption spectrometer. Photoluminescent excitation/emission spectra of HBPPE solution were measured on an F-30 fluorescence spectrophotometer at a scanning speed of 240 nm min^{-1}. Photoluminescent excitation/emission spectra, photoluminescent lifetime and the absolute quantum yield (QY) of pure HBPPE were measured on a UK Edinburgh FLs980 full-featured steady-state/transient fluorescence spectrometer under room temperature. A 340 W xenon lamp was used as the light source. Gel permeation chromatography (GPC) was used to measure the molecular weight and distribution of the HBPPA. The eluent was water. The measurement was performed at a flow rate of 1 mL min^{-1}. The density functional theory (DFT) method at the B3LYP/6-31 G (d) level was used to calculate the energy level of the HBPPE. A transmission electron microscope (TEM) was applied to observe the morphology of HBPPA clusters on a FEI Tecnai G2 F20 microscopy. The measurement was performed under 200 kV, room temperature. The temperature dependency of fluorescence was observed using a Chirascan circular dichroism (CD) spectrometer. Fluorescence microscope images were obtained on a Nikon 80i fluorescence microscope. TGA data was collected on a NETZSCH thermogravimetric analyzer TG 209 F3, Germany. The dynamic light scattering was obtained using Malvern Zetasizer Nano ZS90.

Synthesis

A mixture of TEP (0.15 mol, 27.32 g) and EG (0.24 mol, 14.90 g) was added to a three-necked flask equipped with a condenser, a nitrogen gas inlet and a mechanical stirrer. Then, the mixture was heated to 120 °C, and lasted until stable. During this process, some distillate was distilled off. Afterwards, the mixture was heated to 150 °C to keep the distillation temperature at about 58 °C. The process lasted for about 12 hours. Finally, the product was collected into the vial as the product cooled. The product was dissolved in appropriate ethanol and loaded into the RC dialysis membranes. After 24 hours of dialysis, steaming was carried out to remove the solvent. After steaming, the sample was placed in a vacuum oven overnight. The product HBPPA (named P1) was then obtained.

P2 was synthesized based on the synthesis of P1 by DEP (0.2 mol, 22.01 g) and EG (0.24 mol, 14.90 g). The temperature was kept at 120 °C for 12 h.

P3 was synthesized based on the synthesis of P1 by DEP (0.2 mol, 22.01 g) and Gl (0.16 mol, 14.73 g). The temperature was kept at 80 °C for 8 h.

The detailed data during P1–P3 synthesis are shown in Table S1.†

Results and discussion

In this paper, the HBPPE P1 was synthesized *via* a one-step transesterification polymerization reaction by TEP and EG without a catalyst or solvent. The byproducts were removed through distillation. The synthetic rote of P1 is shown in Scheme 1. To our surprise, P1 could emit bright blue light under UV light. In order to investigate the fluorescence mechanism of HBPPE, the reference polymers, P2 and P3, were also synthesized by DEP and EG or Gl. The synthetic route of P2 and P3 and the possible mechanism are exhibited in Schemes S1 and S2,† respectively.

FTIR study

FTIR spectra of EG, TEP, Gl, DEP, standard ethyl alcohol, standard methyl alcohol, P1–P3, and distillate during the synthesis process are shown in Fig. 1 and S1.† In Fig. 1A, it is clear that the absorption peak of –OH moves from 3522 cm^{-1} for EG to 3337 cm^{-1} for P1. The peak at 1238 cm^{-1} is due to the absorption of P═O groups. The peaks observed at 1018 cm^{-1} and 974 cm^{-1} are due to C–O and P–O groups, respectively. Similarly, the classical absorption peaks of –OH, P═O, C–O and P–O groups appear in FTIR spectra of P2 and P3 (shown in Fig. S1†). In brief, the FTIR spectra indicate that P1–P3 were synthesized successfully. Besides, the FTIR spectrum of distillate during the P1 synthesis process was also detected and shown in Fig. 1B with the standard EA FTIR spectrum. It is obvious that the FTIR spectrum of the distillate during P1 synthesis is identical to that of standard EA, which indicates that the distillate is EA. Similarly, the FTIR spectrum of the distillate during the synthesis of P2 and P3 and standard methyl alcohol, indicates that the distillate is methyl alcohol (displayed in Fig. S1†).

^{1}H NMR and ^{31}P NMR study

To further confirm the P1 structure, ^{1}H NMR spectra of EG, TEP and P1 were observed. As shown in Fig. 2A, the peaks at

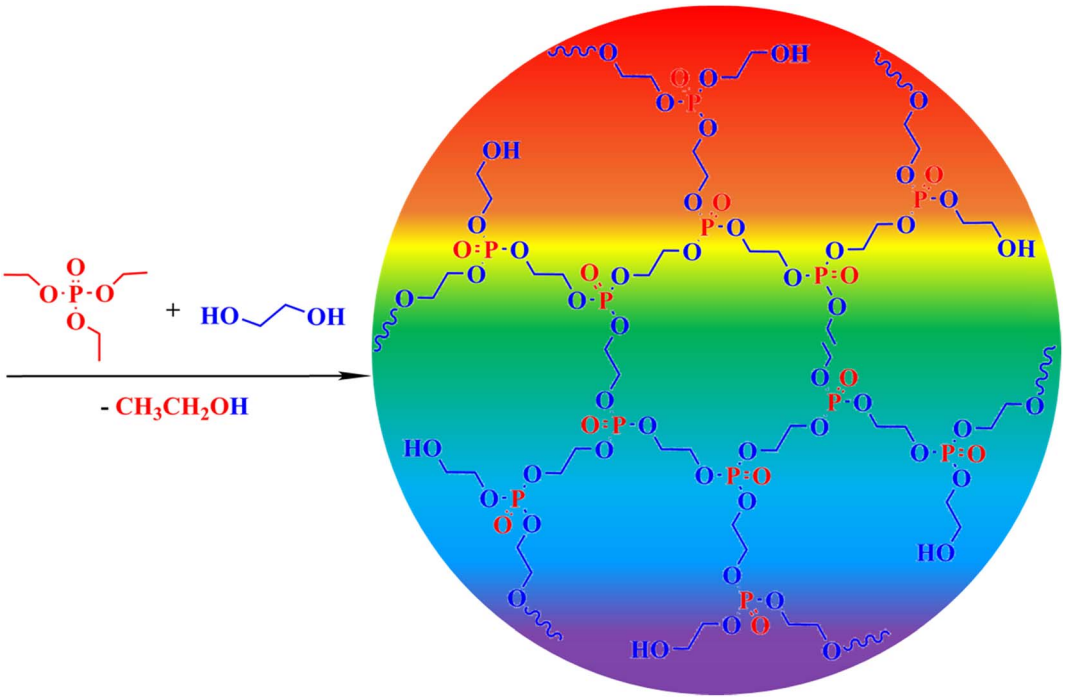

Scheme 1 The synthetic route of P1.

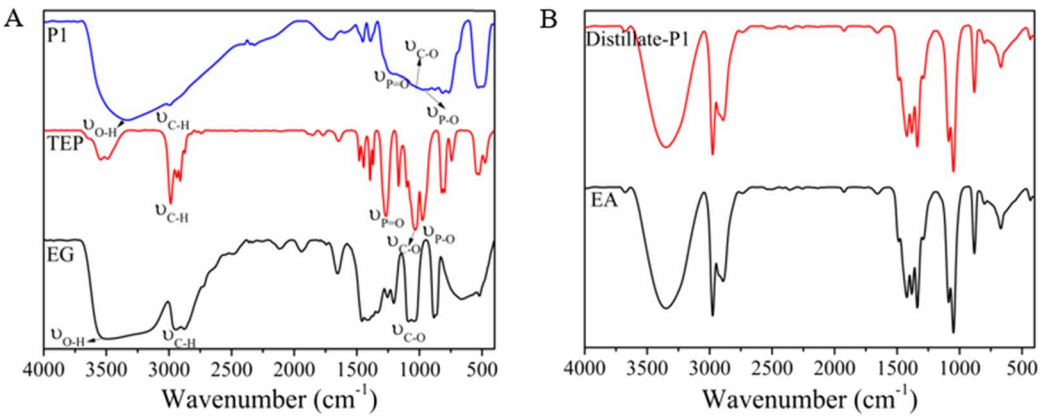

Fig. 1 (A) FTIR spectra of EG, TEP and P1; (B) FTIR spectra of standard ethyl alcohol and distillate during the P1 synthesis process.

1.23–1.26 ppm and 3.97–4.04 ppm are due to –$OCH_2C\underline{H}_3$ and –$C\underline{H}_2$–, respectively. In the EG ^{1}H NMR spectrum, the peaks of –OH and –$C\underline{H}_2$– appear at about 3.39 ppm and 4.28 ppm, respectively. The detailed ^{1}H NMR spectrum is shown in Fig. 2B. The peak observed at about 1.25 ppm belongs to the residual –$C\underline{H}_3$ marked by 5. The peak attributed to –$C\underline{H}_2$– indicated as 3,4 appears at about 4.05–4.18. The peaks at 3.54–3.60 ppm and 3.73–3.78 ppm are due to –OH marked by 1 and –CH_2– marked by 2, respectively. Besides, the ^{31}P NMR spectra of TEP and P1 were also recorded and are shown in Fig. 2C. Combining the ^{1}H NMR and ^{31}P NMR spectra, P1 was synthesized by the designed route. Similarly, ^{1}H NMR spectra of DEP, EG, Cl, P2, P3 and ^{31}P NMR spectra of DEP, P2, and P3 were observed at the same time and displayed in Fig. S2,† which proves that P2 and P3 are synthesized successfully.

GPC study

Furthermore, we measured the molecular weight of P1. The GPC curve is shown in Fig. 3, while the detailed data are shown in Table 1. From Fig. 3, it is obvious that there are two peaks. The two peaks are corresponding to different generations of P1.

In short, FTIR, NMR and GPC results sufficiently demonstrated that P1–P3 were successfully synthesized.

TGA study

To further characterize P1, the TGA of P1 was obtained and is shown in Fig. S3.† P1 showed a main mass loss between 117–

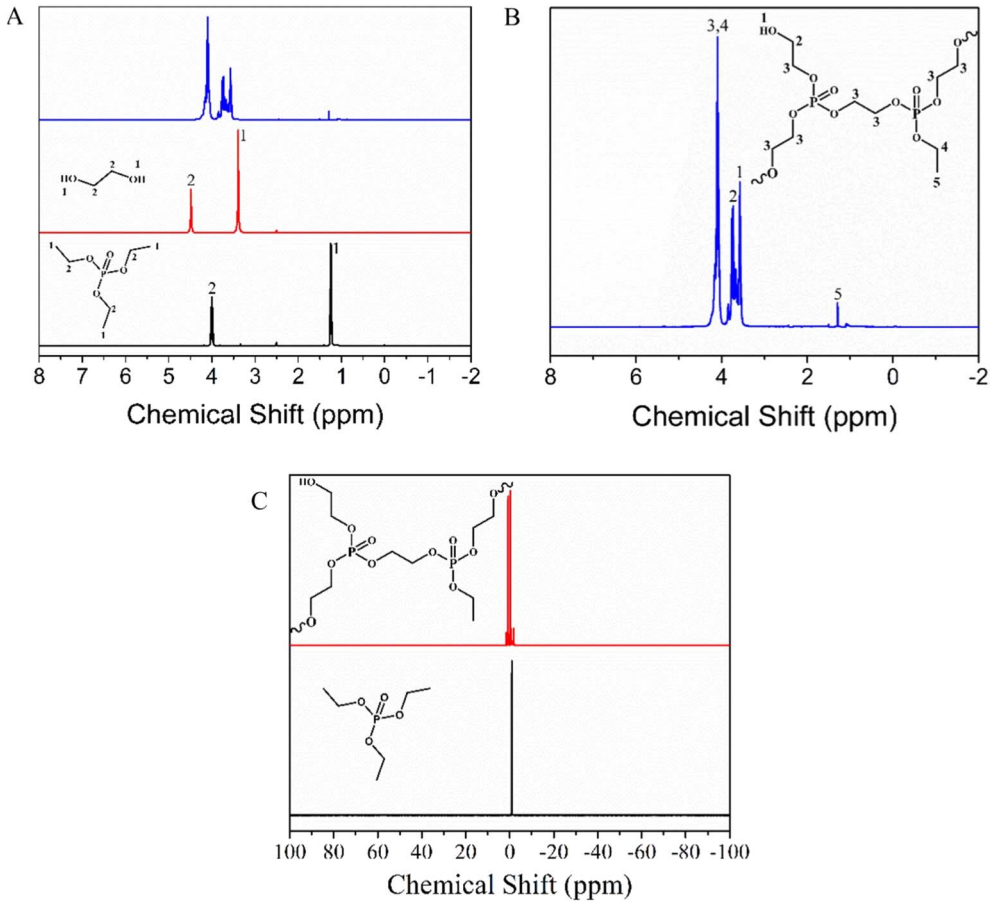

Fig. 2 (A) ^{1}H NMR spectra of TEP, EG and P1; (B) ^{1}H NMR spectra of P1; (C) ^{31}P NMR spectra of TEP and P1.

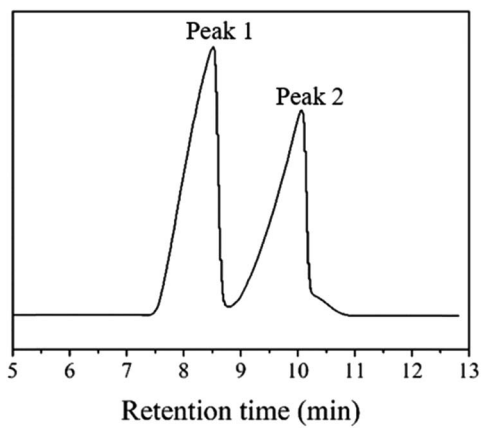

Fig. 3 GPC curve of P1 (eluent: water, narrow standard).

330 °C and a secondary mass loss was between 330–800 °C, with a residual carbon rate of 16.7%.

Optical properties

To our surprise, P1, synthesized using TEP and EG, could emit bright blue light under UV light with AIE character. In order to obtain an insight into the photoluminescence mechanism of HBPPE, P2 (by DEP and EG) and P3 (by DEP and Gl) were synthesized. Unexpectedly, P3, with a hyperbranched structure, could not emit light even in a pure state without any solution. However, P2, with a liner structure, can emit blue light, though the photoluminescence intensity is weaker than that of P1. We are astonished at this phenomenon.

The photoluminescence properties of P1–P3 in an aqueous solution are shown in Fig. 4A. The experimental data indicate a big gap among the photoluminescence intensity of P1, P2 and

Table 1 GPC data for P1

	Number average (M_n)	Weight average (M_w)	Z average (M_z)	(Z + 1) average (M_{z+1})	Polydispersity (PD)	% area
Peak 1	5011	5495	6126	6895	1.10	54.95%
Peak 2	1023	1164	1330	1518	1.14	45.05%

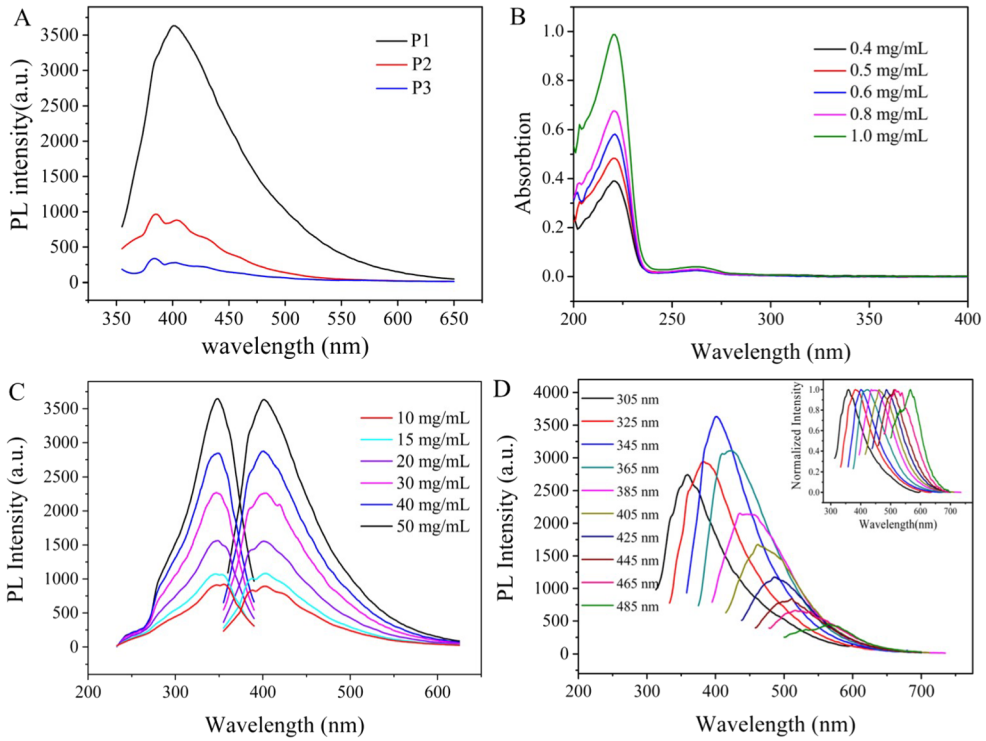

Fig. 4 (A) Photoluminescence spectra of P1 (at 50 mg mL^{-1}), P2 (at 100 mg mL^{-1}) and P3 (pure state); (B) UV-vis absorption spectra of P1 solution at various concentrations; (C) photoluminescence spectra of P1 under different concentration (from 10 mg mL^{-1} to 50 mg mL^{-1}); (D) excitation dependent photoluminescence of P1 aquatic solution at 50 mg mL^{-1} (inset: normalized emission).

P3, resulting in the difficulty in obtaining photoluminescence spectra of P1–P3 under the same concentration. Hence, we observed the photoluminescence spectra of P1 at 50 mg mL^{-1}, P2 at 100 mg mL^{-1} and P3 in the pure state. It is evident that the photoluminescence intensity of P1 is the strongest among the three polymers. Contrary to the general opinion, P3 can hardly emit light under UV. Though the photoluminescence intensity of P2 is weaker than that of P1, it is stronger than that of P3. It is considered that a hyperbranched structure is not a sufficient element to decide whether the polymer can emit light or not. Besides the hyperbranched structure, the structure of the polymer itself is the necessary element. Compared to the structure of P1 and P3, the difference exists in the center. P1, centering in phosphoryl groups, has more advantages in self-assembly, resulting from the special band angle. That will prompt the formation of an electronic delocalization system, where the energy stored is the origin of visible light emission. However, in P3, centering in carbon, the self-assembly is limited, resulting in the inhibition of visible light emission.

The UV absorption spectra of the P1 aqueous solution were detected under different concentrations. As shown in Fig. 4B, the peak at about 202 nm is attributed to the n → π* electronic transitions between the P═O, P–O and C–O groups. While the peak belonged to the π → π* electronic transitions between the P═O groups appear at around 221 nm. Especially, the peak that appeared at about 280 nm is attributed to the through-space conjugation formed by P═O and oxy groups through the self-assembly of P1, which is important evidence for the formation of an electronic delocalization system. It is obvious that the absorption intensity is enhanced along with the increase of the P1 aqueous solution concentration. This is attributed to the enhanced P═O and oxy group aggregation caused by the increase in the concentration of P1 solution, resulting in more easy triggering of electronic transitions.

Surprisingly, the photoluminescence intensity of P1 increased along with the increase of P1 solution concentration, showing a distinct AIE character. In addition, the photoluminescence intensity of P1 with ethyl alcohol as a good solvent and petroleum ether as a bad solvent is shown in Fig. S4.† The photoluminescence intensity increases along with the increase of petroleum ether volume fraction, indicating AIE character. The detailed photoluminescence spectra are shown in Fig. 4C. The Stoke shifts are shown in Table S2.† It is obvious that there are three excitation bands at around 278 nm, 345 nm and 355 nm while the emission bands appear at 385 nm, 401 nm and 420 nm, respectively. It is obvious that the excitation band at about 348 nm is the main peak, which is attributed to the electronic delocalization system, while the band at 27 nm belongs to the molecular skeleton of P1. The three emission bands originate from various clusters with different sizes. As the concentration increases, the strength of intramolecular and intermolecular hydrogen bonds is enhanced, resulting in better self-assembly. This is attributed to the formation of through-space conjugation, resulting in the formation of an electronic delocalization system, which is attributed to photoluminescence emission.

Meanwhile, it is found that the emission band is closely related to the excitation wavelength. The detailed photoluminescence spectra of P1 under different excitation wavelengths are shown in Fig. 4D. It is obvious that the highest photoluminescence intensity appears at 345 nm. There is an obvious red shift as the increase of the excitation wavelength, which is shown in the normalized photoluminescence spectra. The red shift is a result of the clusters with different sizes and the formed electronic delocalization system, which can be proved by TEM and DFT calculation results. Then, the commission internationale de L'Eclairage (CIE) chromaticity coordinates of P1 were calculated based on the photoluminescence spectra under different excitation wavelengths and are shown in Fig. 5A. It is obvious that P1 can emit blue, cyan, green and yellow light, covering almost the whole visible light range. Besides, we also get the photoluminescence photo using a fluorescence microscope under different excitation wavelengths, which is shown in Fig. 5B. Amazingly, pure P1 can emit red light under the excitation of 510–560 nm light. The water-soluble and multicolor-emitted P1 has a wonderful prospect in bioimaging and visual drug delivery.

Afterwards, the photoluminescence spectra, photoluminescence lifetime and absolute QY of pure HBPPE were obtained. From Fig. 6A, it is clear that the excitation bands appear at 372–394 nm, while the emission bands appear at 421 nm, 440 nm and 461 nm. Compared with the photoluminescence spectra of the P1 solution, there is an obvious red shift both in excitation and emission bands. This is due to the formed electronic delocalization system, which can reduce the needed energy of excitation. The absolute photoluminescence quantum yield of P1 is shown in Fig. 6B. The QY is 22.42%, relatively high among nonconventional AIE materials. The transient photoluminescence decay curve of P1 is shown in Fig. 6C. By calculation, the lifetime is 12.82 μs (τ_1 = 1.1939 μs (3.09%), τ_2 = 12.85 μs (96.91%)), which suggests the first long-lived material without aromatic structure. It is believed that phosphorus incorporation can sufficiently improve the photoelectric properties of the photoelectric materials are due to the novel electronic and optical properties of phosphorus. Besides, the high QY and lifetime are related to the special covalent-crystal-like spatial structure of P1, which can be proved by the DFT calculation results. Besides, the quantum yield and lifetime of P1 solution at 10 mg mL^{-1} and 50 mg mL^{-1} were studied and the data are shown in Fig. S5.† The QY of P1 at 10 mg mL^{-1} and 50 mg mL^{-1} are 3.84%, and 4.39%, respectively. The lifetime are 13.10 μs (τ_1 = 3.23 μs (24.38%), τ_2 = 13.84 μs (75.62%)) and 11.22 μs (τ_1 = 3.34 μs (29.78%), and τ_2 = 12.14 μs (70.22%)), respectively. At the pure state, the highest quantum yield was observed. The values of the radiative (k_r) and non-radiative (k_{nr}) rates as a function of concentration were calculated and are shown in Table S3.† At the pure state, the highest k_r was obtained.

Compared with the other nontraditional AIE materials, especially poly(ester)s, the incorporation of phosphorus markedly improves the photoluminescence properties on photoluminescence intensity, QY and lifetime. The signal improvement in lifetime was not only due to the novel electronic and optical properties of phosphorus but also resulted from the special covalent-crystal-like spatial structure of P1.

TEM study

In order to obtain an insight into the photoluminescence mechanism of P1, we observed the morphology of P1 under different concentrations. The TEM photo is shown in Fig. 7. From Fig. 7A, it is obvious that P1 assembles into hollow spheres with a small size at the concentration of 10 mg mL^{-1}.

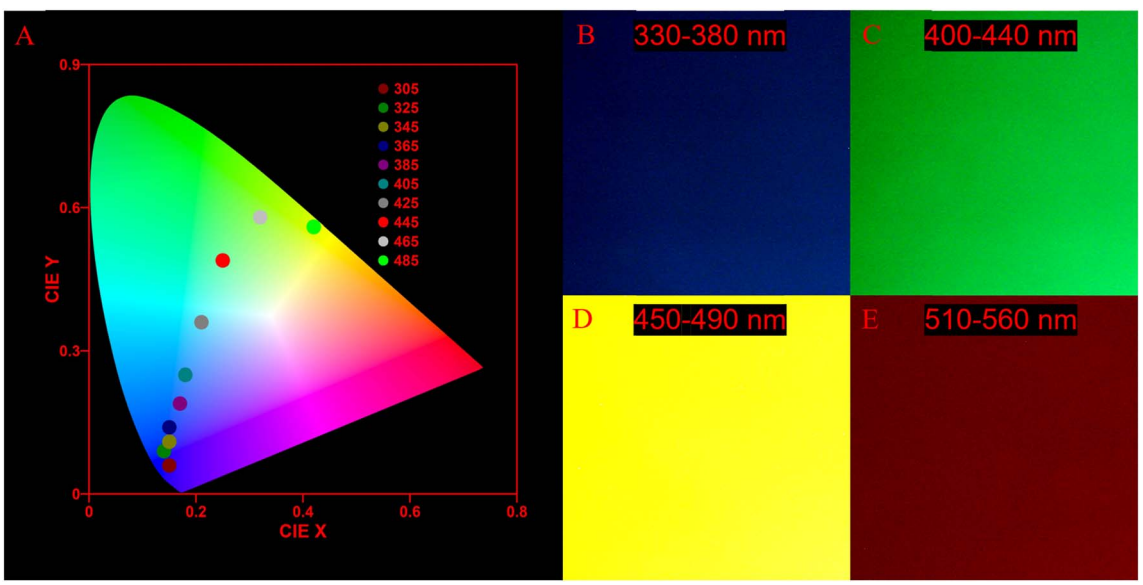

Fig. 5 (A) CIE chromaticity coordinates obtained from the emission spectra of P1 at 20 mg mL^{-1}; (B) fluorescence microscope image of pure P1 under the light filter of UV-2A (Ex 330–380 nm, DM 400, DA 420); (C) fluorescence microscope image of pure P1 under the light filter of BV-2A (Ex 400–440 nm, DM 455, DA 470); (D) fluorescence microscope image of pure P1 under the light filter of B-2A (Ex 450–490 nm, DM 505, DA 520); (E) fluorescence microscope image of pure P1 under the light filter of G-2A (Ex 510–560 nm, DM 575, DA 590).

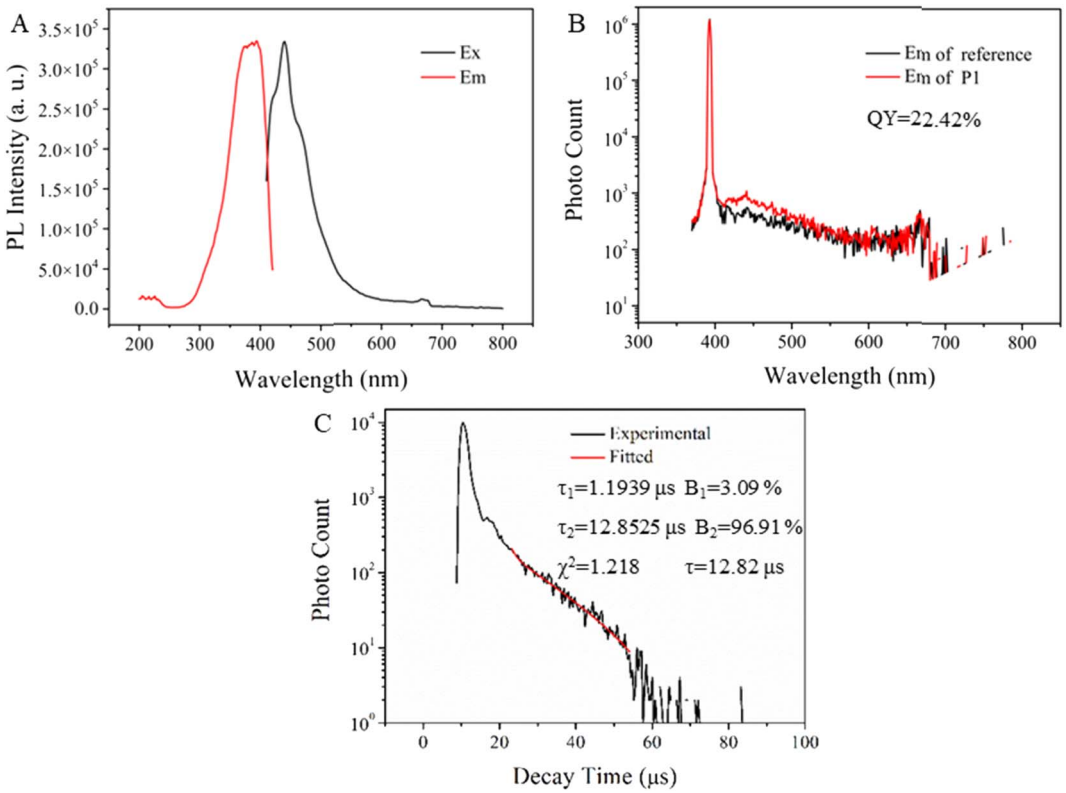

Fig. 6 (A) Excitation spectra (Ex, monitored at $\lambda_{em} = 440$ nm) and emission spectra (Em, excited at $\lambda_{ex} = 394$ nm) of P1; (B) absolute photoluminescence quantum yield of P1 excited at 394 nm; (C) transient photoluminescence decay curve of P1 at 440 nm after excitation at 399 nm.

However, at 50 mg mL^{-1}, P1 assembles into solid spherical with larger but uneven size. Dynamic light scattering also shows that the particle size increases with the increase in concentration (Fig. S6†). That is to say, self-assembly is better in the concentrated solution than in the dilute solution. This is because the distance between molecules is shorter in the concentrated solution, which strengthens the intermolecular hydrogen bonds. Then, the molecules will form larger and harder conformations. In this state, non-radiative transition is limited. Instead, the energy is consumed through radiation transition, resulting in the formation of photoluminescence. That is why the photoluminescence intensity in the concentrated solution is stronger than in a dilute solution. Besides, the uneven size is one season for the multicolor emission.

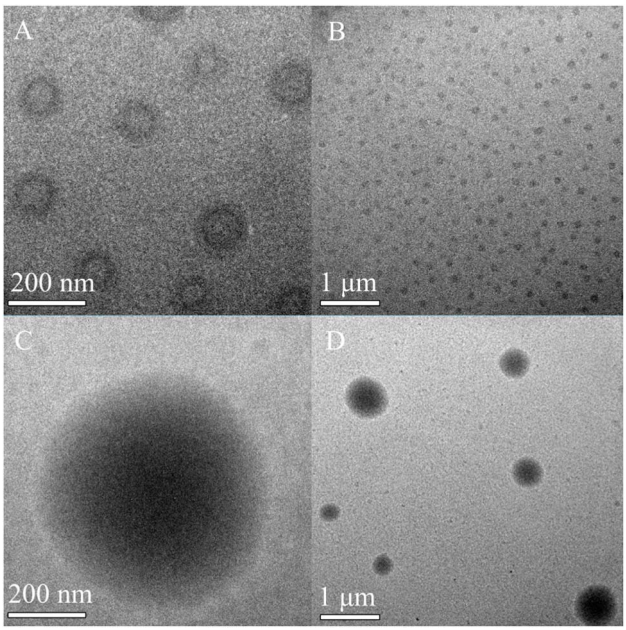

Fig. 7 Micrograph of P1 self-assembly morphology in ethanol with the concentration at 10 mg mL^{-1} (A and B) and 50 mg mL^{-1} (C and D).

Theoretical calculations

In order to recover the photoluminescence mechanism from the micro perspective, density functional theory (DFT) was used to calculate the energy at the optimized conformations. For the simplification of the calculation of HBPPE, the energy levels of the first generation molecules of HBPPE increasing from one to four were calculated, which is applied for the simulation of the change of concentration. Besides, the energy levels of first to third-generation molecules of P1 were calculated to simulate the change in the molecular weight. The optimized conformation of first-generation P1 with a different number of molecules, first-generation P3 with a different number of molecules, and different generation P1 with one molecule are shown in Fig. 8, 9 and S3, S4.† The HOMO–LUMO energy levels of P1 and P3 with different molecules, and P1 with different generations were also calculated and the results are shown in Table S3.†

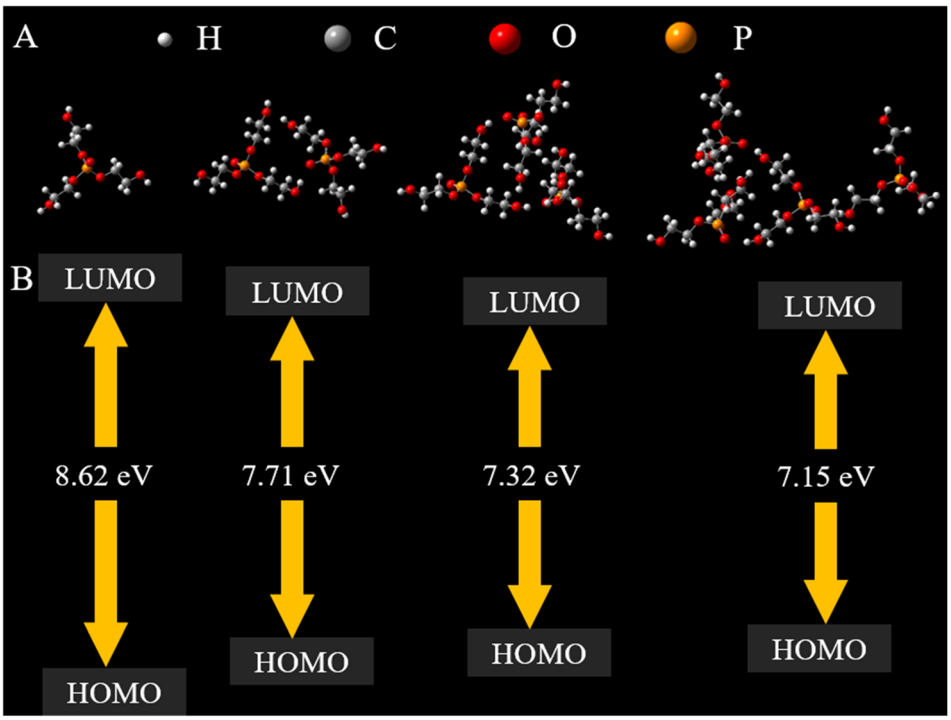

Fig. 8 (A) Optimized conformations of the first generation P1 with molecules increase from 1 to 4; (B) the schematic diagram of HOMO–LUMO at the optimized conformations of the first generation P1 with molecules increase from 1 to 4.

It is distinct that the energy gap is reduced with the increase in the number of P1 molecules. That is to say, the energy gap is reduced with the increment in the concentration of the P1 solution. The lower energy gap is in favour of excitation and will absorb more energy from excitation light, which means that more energy is stored in the excitation state. Then, the energy assumed in the formation of radiative transition increases, resulting in the increment of photoluminescence intensity, which is consistent with the experimental results as the concentration increases. Besides, it can be seen from the optimized conformations of P1 with 1–4 molecules that a more tight conformation is formed with the increase in the number of P1 molecules due to the intramolecular and intermolecular hydrogen bonds (1.811 Å, 1.894 Å, 1.807 Å, 1.833 Å, 1.916 Å, and 1.816 Å, as shown in Fig. 9A). At this state, through-space conjugation is formed due to the interactions between O···O and P═O (2.759 Å, 2.846 Å, 2.850 Å, 2.746 Å, and 2.802 Å, as exhibited in Fig. 9B), and then it is followed with the formation of the electron delocalization system (as displayed in Fig. 9C and D). The formation of through-space conjugation results in a relatively high QY. While the strong fluorescence emission and multicolor emission are due to the formed electron delocalization system.

Moreover, with the increase of P1 generation, the energy gap is also reduced. Similarly, this suggests an increment in photoluminescence intensity, which is consistent with the relationship between molecular weight and photoluminescence intensity. More importantly, a covalent-crystal-like conformation is gradually formed with P1 generation increasing, which makes the through-space conjugation formed by self-assembly similar to the conjugation of aromatic materials. As a result, it is supposed that the interactions between the formed rings in space are the origin of the long-lived lifetime.

Compared to the energy gaps of P1 and P3 at the same molecular number, it is evident that the energy gap of P3 is unexpectedly lower than that of P1. However, P3 cannot emit any light under excitation. Compared to the structure and optimized conformations of P1 and P3 (shown in Fig. S7 and S8†), the difference lies in the bond angle between O–P–O, which results in the covalent-crystal-like conformations of P1, while the covalent-crystal-like conformation is just the origin of the photoluminescence.

Temperature dependency

Furthermore, we found that temperature can influence the fluorescence intensity of P1. The photoluminescence spectra of P1 under different temperatures are shown in Fig. S9† (at 50 mg mL^{-1}). It is apparent that the photoluminescence intensity decreases with the increase in temperature. That is because the increased temperature will speed up the Brownian motion, which results in the energy assumed in nonradiative transition increased, while that through radiative transition is reduced. Then, the photoluminescence emission is weaker. This discovery provides an effective and concise means for visual detection of temperature through photoluminescence.

Ion probe

For checking whether the hyperbranched polyphosphate can be used as a metal ions probe, the photoluminescence spectra of P1 with different kinds of metal ions (Na^+, Hg^{2+}, Cd^{2+}, Al^{3+},

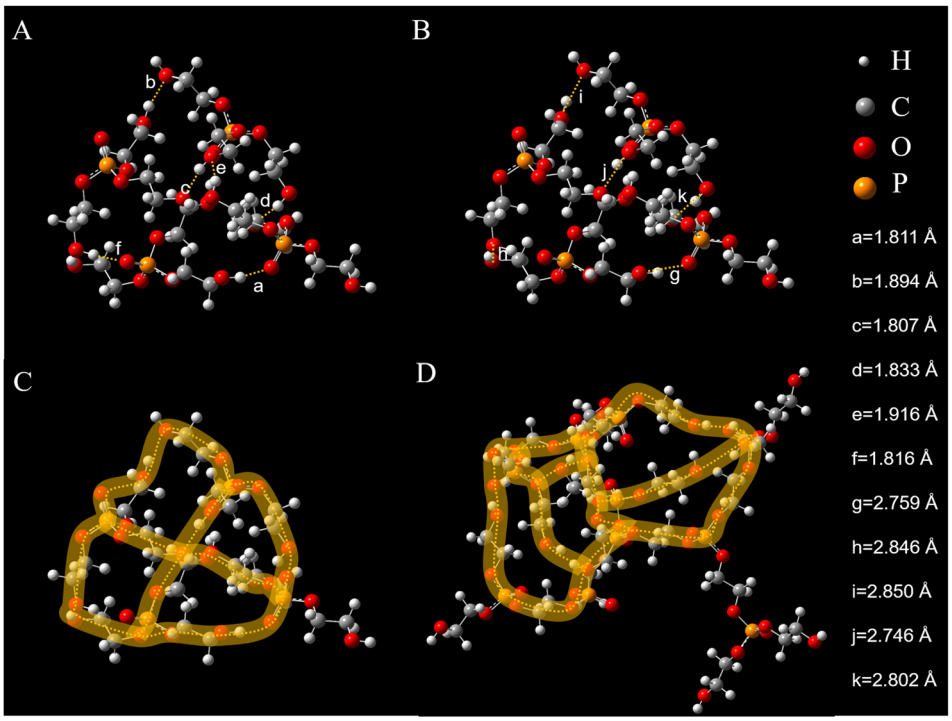

Fig. 9 (A) The accumulation of four P1 first-generation molecules induced by H···O intermolecular interactions; (B) intramolecular and intermolecular O···O interactions between four P1 molecules; (C) schematic diagram of the through-space conjugation for P1; and (D) schematic diagram of the through-space conjugation for P1.

NH_4^+, Zn^{2+}, Cu^{2+}, and Fe^{3+}) were measured (Fig. S10A†). It is obvious that the addition of Fe^{3+} caused the most distinct effect on the photoluminescence intensity. That can be attributed to the formation of the P1–Fe^{3+} complex, leading to the intramolecular charged transfer from Fe^{3+} to P1. Besides, the photoluminescence can be recovered when adding ethylenediaminetetraacetic acid. The photoluminescence intensity of P1 decreases gradually with the increase of Fe^{3+} concentration. Moreover, the fluorescence of P1 is almost quenched when Fe^{3+} concentration reaches 1×10^{-4} mol L^{-1}. The calibration curve depicts $-\ln(P/P_0)$ response to different concentrations of Fe^{3+} in P1 solution, where P_0 and P are photoluminescence intensities of P1 in the absence and presence of Fe^{3+}. $-\ln(P/P_0)$ presents a linear response to Fe^{3+} concentration in the range of 1×10^{-6} to 1×10^{-4} mol L^{-1}, with a correlation coefficient of $R^2 = 0.9962$ (Fig. S10B†). P1 has the potential to be used as a biological photoluminescence probe for Fe^{3+}.

Conclusion

In this study, a novel kind of hyperbranched/liner PPE P1–P3 was synthesized through TEP, DEP, EG and Gl by transesterification polycondensation reaction without a catalyst. Surprisingly, the obtained HBPPE P1 could emit bright blue photoluminescence under UV light and show significant AIE character. While P3 can hardly emit any light. Experimental and theoretical calculations by DFT reveal that P1 will assemble into a sphere through intramolecular and intermolecular hydrogen bonds. The hydrogen bonds lead to the formation of covalent-crystal-like conformation. Then, through-space conjugation is formed due to the cooperation of hydroxyl, P═O and P–O groups, resulting in the formation of an electronic delocalization system, which is in favor of photoluminescence emission. The calculations of P1 and P3 reveal that the fluorescence originates from the covalent-crystal-like structure. Amazingly, the average phosphorescence lifetime of P1 is 12.82 μs with a quantum yield of up to 22.4%, suggesting the first RTP material without aromatic structure. Besides, P1 shows an obvious red-shift along with the excitation wavelength increasing, the emission light covers almost all the visible light region. To be noted, the fluorescence intensity of HBPPE was sensitive to the temperature. This study not only enriches the species of nonconventional multicolor emission AIE materials but also provides a concise method for the synthesis of HBPPE. Most importantly, this research supplies the possibility for RTP materials without rare elements or bulky aromatic or conjugated units, which is a great progress on RTP AIE materials.

Data availability

We confirm that the data supporting the findings of this study are available within the main article and ESI.†

Author contributions

The manuscript was written through the contributions of all authors. All authors have given approval to the final version of the manuscript.

Conflicts of interest

There are no conflicts to declare.

References

1 Z. Liao, Y. Wang, Y. Lu, R. Zeng, L. Li, H. Chen, Q. Song, K. Wang and J. Zheng, Covalently hybridized carbon dots@mesoporous silica nanobeads as a robust and versatile phosphorescent probe for time-resolved biosensing and bioimaging, *Analyst*, 2024, 1473–1480, DOI: 10.1039/D3AN01935G.

2 B. T. Luppi, W. L. Primrose and Z. M. Hudson, Polymer Dots with Delayed Fluorescence and Tunable Cellular Uptake for Photodynamic Therapy and Time-Gated Imaging, *Angew. Chem., Int. Ed.*, 2024, **63**(17), e202400712, DOI: 10.1002/anie.202400712.

3 Z. Zhao, R. Du, X. Feng, Z. Wang, T. Wang, Z. Xie, H. Yuan, Y. Tan and H. Ou, Regulating Triplet Excitons of Organic Luminophores for Promoted Bioimaging, *Curr. Med. Chem.*, 2024, DOI: 10.2174/0109298673301552240305064259.

4 J. Chatterjee, A. Chatterjee, R. Tanwar, P. Panwaria, S. Saikia, M. D. Ambhore, P. Mandal and P. Hazra, Activation of TADF in Photon Upconverting Crystals of Dinuclear Cu(I)-Iodide Complexes by Ligand Engineering, *J. Phys. Chem. Lett.*, 2024, 6069–6080, DOI: 10.1021/acs.jpclett.4c01122.

5 J. M. Jacob and M. K. Ravva, Impact of Surrounding Environment on Hot-Exciton Based Organic Emitters for TADF Applications, *ChemPhotoChem*, 2024, e202400073, DOI: 10.1002/cptc.202400073.

6 C. W. Lee and J. Y. Lee, Above 30% External Quantum Efficiency in Blue Phosphorescent Organic Light-Emitting Diodes Using Pyrido[2,3-b]indole Derivatives as Host Materials, *Adv. Mater.*, 2013, 5450–5454, DOI: 10.1002/adma.201301091.

7 C. Adachi, M. A. Baldo, M. E. Thompson and S. R. Forrest, Nearly 100% internal phosphorescence efficiency in an organic light-emitting device, *J. Appl. Phys.*, 2001, 5048–5051, DOI: 10.1063/1.1409582.

8 G. Qu, Y. Zhang and X. Ma, Recent progress on pure organic room temperature phosphorescence materials based on host-guest interactions, *Chin. Chem. Lett.*, 2019, 1809–1814, DOI: 10.1016/j.cclet.2019.07.042.

9 S. M. Parke and E. Rivard, Aggregation Induced Phosphorescence in the Main Group, *Isr. J. Chem.*, 2018, 915–926, DOI: 10.1002/ijch.201800039.

10 N. Gan, H. Shi, Z. An and W. Huang, Recent Advances in Polymer-Based Metal-Free Room-Temperature Phosphorescent Materials, *Adv. Funct. Mater.*, 2018, 1802657, DOI: 10.1002/adfm.201802657.

11 P. Parimita Dash, A. Kumar Ghosh, P. Mohanty, R. Behura, S. Behera, B. R. Jali and S. K. Sahoo, Advances on fluorescence chemosensors for selective detection of water, *Talanta*, 2024, 126089, DOI: 10.1016/j.talanta.2024.126089.

12 P. Coghi and C. Coluccini, Literature Review on Conjugated Polymers as Light-Sensitive Materials for Photovoltaic and Light-Emitting Devices in Photonic Biomaterial Applications, *Polymers*, 2024, 1407, DOI: 10.3390/polym16101407.

13 A. A. Bhosle, M. Banerjee and A. Chatterjee, Aggregation-induced emission-active azines for chemosensing applications: a five-year update, *Sens. Diagn.*, 2024, 745–782, DOI: 10.1039/d3sd00348e.

14 W. Zhang Yuan and Y. Zhang, Nonconventional macromolecular luminogens with aggregation-induced emission characteristics, *J. Polym. Sci., Part A: Polym. Chem.*, 2017, 560–574, DOI: 10.1002/pola.28420.

15 D. A. Tomalia, B. Klajnert-Maculewicz, K. A. M. Johnson, H. F. Brinkman, A. Janaszewska and D. M. Hedstrand, Non-traditional intrinsic luminescence: inexplicable blue fluorescence observed for dendrimers, macromolecules and small molecular structures lacking traditional/conventional luminophores, *Prog. Polym. Sci.*, 2019, 35–117, DOI: 10.1016/j.progpolymsci.2018.09.004.

16 Y. Feng, T. Bai, H. Yan, F. Ding, L. Bai and W. Feng, High Fluorescence Quantum Yield Based on the Through-Space Conjugation of Hyperbranched Polysiloxane, *Macromolecules*, 2019, 3075–3082, DOI: 10.1021/acs.macromol.9b00263.

17 L. Bai, H. Yan, T. Bai, Y. Feng, Y. Zhao, Y. Ji, W. Feng, T. Lu and Y. Nie, High Fluorescent Hyperbranched Polysiloxane Containing β-Cyclodextrin for Cell Imaging and Drug Delivery, *Biomacromolecules*, 2019, 4230–4240, DOI: 10.1021/acs.biomac.9b01217.

18 S. Niu, H. Yan, Z. Chen, S. Li, P. Xu and X. Zhi, Unanticipated bright blue fluorescence produced from novel hyperbranched polysiloxanes carrying unconjugated carbon–carbon double bonds and hydroxyl groups, *Polym. Chem.*, 2016, 3747–3755, DOI: 10.1039/C6PY00654J.

19 L. Yuan, H. Yan, L. Bai, T. Bai, Y. Zhao, L. Wang and Y. Feng, Unprecedented Multicolor Photoluminescence from Hyperbranched Poly(amino ester)s, *Macromol. Rapid Commun.*, 2019, 1800658, DOI: 10.1002/marc.201800658.

20 D. Wu, Y. Liu, C. He and S. H. Goh, Blue Photoluminescence from Hyperbranched Poly(amino ester)s, *Macromolecules*, 2005, 9906–9909, DOI: 10.1021/ma051407x.

21 Y. Lin, J.-W. Gao, He-W. Liu and Y.-S. Li, Synthesis and Characterization of Hyperbranched Poly(ether amide)s with Thermoresponsive Property and Unexpected Strong Blue Photoluminescence, *Macromolecules*, 2009, 3237–3246, DOI: 10.1021/ma802353f.

22 Q. Zhou, B. Cao, C. Zhu, S. Xu, Y. Gong, W. Z. Yuan and Y. Zhang, Clustering-Triggered Emission of Nonconjugated Polyacrylonitrile, *Small*, 2016, 6586–6592, DOI: 10.1002/smll.201601545.

23 K. Kajuzyáski, J. Libiszowski and St. Penczek, A New Class of Synthetic Polyelectrolytes. Acidic Polyesters of Phosphoric Acid,(Poly(hydroxyalkylene phosphates)), *Macromolecules*, 1976, 365–367.

24 S.-W. Huang and R.-X. Zhuo, Recent Advances in Polyphosphoester and Polyphosphoramidate-Based Biomaterials, *Phosphorus, Sulfur Silicon Relat. Elem.*, 2008, 340–348, DOI: 10.1080/10426500701734620.

25 H. Wang, J. He, M. Zhang, K. C. Tam and P. Ni, A new pathway towards polymer modified cellulose nanocrystals via a "grafting onto" process for drug delivery, *Polym. Chem.*, 2015, 4206–4209, DOI: 10.1039/C5PY00466G.

26 Z. Ergul Yilmaz and C. Jérôme, Polyphosphoesters: New Trends in Synthesis and Drug Delivery Applications, *Macromol. Biosci.*, 2016, 1745–1761, DOI: 10.1002/mabi.201600269.

27 Z.-Y. Wang, X.-W. Li, J.-N. Li, G.-M. Li and J.-Q. Tao, Synthesis of poly(lactic acid)-poly(phenyl phosphate) via direct polycondensation and its characterization, *J. Polym. Res.*, 2009, 255–261, DOI: 10.1007/s10965-008-9224-0.

28 K. Kishore, P. Kannan and K. Iyanar, Synthesis, characterization, and fire retardancy of ferrocene containing polyphosphate esters, *J. Polym. Sci., Part A: Polym. Chem.*, 1991, 1039–1044, DOI: 10.1002/pola.1991.080290711.

29 K. Kishore and P. Kannan, Synthesis, spectral, thermal, and flammability studies of phenolphthalein polyphosphate esters, *J. Polym. Sci., Part A: Polym. Chem.*, 1990, 3481–3486, DOI: 10.1002/pola.1990.080281223.

30 L. Ding, L. Lin, C. Wang, J. Qiu and Z. Zhu, Facile synthesis of linear–hyperbranched polyphosphoesters via one-pot tandem ROMP and ADMET polymerization and their transformation to architecturally defined nanoparticles, *J. Polym. Sci., Part A: Polym. Chem.*, 2015, 964–972, DOI: 10.1002/pola.27524.

31 T. Steinbach, C. Wahlena and F. R. Wurm, Poly(phosphonate)-mediated Horner – Wadsworth – Emmons reactions, *Polym. Chem.*, 2015, 1192–1202.

32 K. Malzahn, F. Marsico, K. Koynov, K. Landfester, C. K. Weiss and F. R. Wurm, Selective Interfacial Olefin Cross Metathesis for the Preparation of Hollow Nanocapsules, *ACS Macro Lett.*, 2014, 40–43, DOI: 10.1021/mz400578e.

33 C.-S. Xiao, Y.-C. Wang, J.-Z. Du, X.-S. Chen and J. Wang, Kinetics and Mechanism of 2-Ethoxy-2-oxo-1,3,2-dioxaphospholane Polymerization Initiated by Stannous Octoate, *Macromolecules*, 2006, 6825–6831, DOI: 10.1021/ma0615396.

34 D.-P. Chen and J. Wang, Synthesis and Characterization of Block Copolymer of Polyphosphoester and Poly(ε-caprolactone), *Macromolecules*, 2006, 473–475, DOI: 10.1021/ma0517852.

35 Y. C. Wang, S. Y. Shen, Q. P. Wu, D. P. Chen, J. Wang, G. Steinhoff and N. Ma, Block Copolymerization of -Caprolactone and 2-Methoxyethyl Ethylene Phosphate Initiated by Aluminum Isopropoxide: Synthesis, Characterization, and Kinetics, *Macromolecules*, 2006, 8992–8998, DOI: 10.1021/ma061821c.